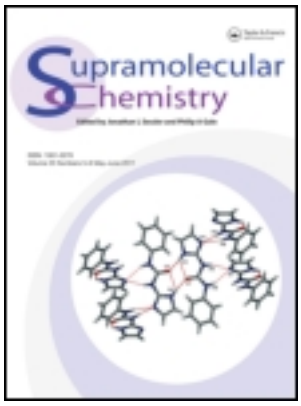

Supramolecular Chemistry

Publication details, including instructions for authors and subscription information:
http://www.tandfonline.com/loi/gsch20

Molecular motion in zinc hydrazone grid complexes

Manisha Dutta [a], Meisam Movassat [b], David J.R. Brook [b], Allen Oliver [c] & Don Ward [d]

[a] Department of Chemistry and Biochemistry, University of Detroit Mercy, Detroit, MI, USA

[b] Department of Chemistry, San Jose State University, San Jose, CA, USA

[c] Department of Chemistry and Biochemistry, University of Notre Dame, Notre Dame, IN, USA

[d] Department of Chemistry and Biochemistry, Michigan State University, East Lansing, MI, USA

Available online: 04 Jul 2011

To cite this article: Manisha Dutta, Meisam Movassat, David J.R. Brook, Allen Oliver & Don Ward (2011): Molecular motion in zinc hydrazone grid complexes, Supramolecular Chemistry, 23:9, 632-643

To link to this article: http://dx.doi.org/10.1080/10610278.2011.593626

Supramolecular Chemistry
Vol. 23, No. 9, September 2011, 632–643

Molecular motion in zinc hydrazone grid complexes

Manisha Dutta[a], Meisam Movassat[b], David J.R. Brook[b]*, Allen Oliver[c] and Don Ward[d]

[a]*Department of Chemistry and Biochemistry, University of Detroit Mercy, Detroit, MI, USA;* [b]*Department of Chemistry, San Jose State University, San Jose, CA, USA;* [c]*Department of Chemistry and Biochemistry, University of Notre Dame, Notre Dame, IN, USA;* [d]*Department of Chemistry and Biochemistry, Michigan State University, East Lansing, MI, USA*

(*Received 13 May 2010; final version received 17 May 2011*)

Four new grid forming hydrazone ligands substituted with methoxy and dimethylamino groups were synthesised. Combination of these ligands with zinc triflate in acetonitrile resulted in self-assembly to form grids as indicated by ^{1}H NMR and ES-MS. ^{1}H NMR also showed thermally induced rotation of the intercalated phenyl ring in both the new grids, and in three previously reported grid compounds. Of these seven, five were amenable to study by variable temperature ^{1}H NMR. Though the observed rates varied by more than an order of magnitude depending upon ligand structure and level of deprotonation, activation energies were similar (~60 kJ/mol) for all complexes studied. This suggests a model in which dissociation of the central pyrimidine ligand precedes phenyl group rotation with an enthalpy of dissociation near zero. The rate of rotation of the phenyl ring increases with an introduction of electron-donating substituents on the phenyl ring, possibly due to an increased repulsion between π systems.

Keywords: self-assembly; hydrazones; dynamic-^{1}H NMR; zinc

Introduction

Self-assembly is an attractive way to make complex functional molecular architectures through the recognition and binding of complementary molecules. Though progress has been made on design criteria for self-assembling systems, the dynamic process of self-assembly has been studied in far less detail. Self-assembled systems are often presented as crystal structures or mass spectral peaks; however, dynamic processes, such as the ability to exchange, dissociate and bind components, are essential to the process of assembly and the attainment of a thermodynamic minimum (*1*). Mechanistic studies are also important in the understanding of general supramolecular phenomena such as self-organisation – the ability of self-assembling systems to recognise and associate in the presence of other competing interactions – and specific dynamic phenomena such as the metal ion-driven coiling and uncoiling motion of ligands (*2*), solvent-driven exchange between 'grid'-type and 'pincer'-type complexes (*3*) and the selective formation of grid ligands from combinatorial libraries (*4*, *5*). Some of these effects can be driven by the changes in equilibrium constant as small as a factor of 10 (*6*).

Recent results have looked at component exchange in metal-coordinated polygons via isotope exchange (*7*) and hydrogen-bonded arrays via fluorescent resonant energy transfer (*8–10*). These systems involve relatively simple interactions between supramolecular components. The formation of grid complexes from polypyridyl ligands is particularly interesting because of the interplay between metal binding and π-stacking interactions. The latter are often described as supporting the formation of the grid (*11*, *12*), though little quantitative evidence has been provided.

Recent work in self-assembled grids has utilised the hydrazone link as a substitute for a pyridine ring. This has enormous synthetic advantages but further changes the interactions involved in the grid assembly. Unlike a pyridine ring which has a basic nitrogen lone pair but an electron-deficient π system, hydrazones have both a basic nitrogen and an electron rich π system isoelectronic with an allyl anion. Hydrazones with a free NH group frequently become more acidic on metal binding; deprotonation of the hydrazone NH increases the donor characteristics of the ligand and increases electron density on the metal ion (*13*). Deprotonation of hydrazones has been used to both drive self-assembly (*14*) and control self-assembly through the manipulation of the redox chemistry of the metal ion (*15*, *16*). We have also shown that under some circumstances deprotonation of a hydrazone ligand changes the coordination environment such that a phenyl ring that is rigidly intercalated between ligands in the solid state can undergo restricted rotation in solution (*14*). Lehn and co-workers have noted that phenyl rotation in polypyridyl grid systems could be used to

*Corresponding author. Email: dbrook@science.sjsu.edu

ISSN 1061-0278 print/ISSN 1029-0478 online

http://dx.doi.org/10.1080/10610278.2011.593626
http://www.tandfonline.com

investigate ligand dissociation (*11*), though to our knowledge no further study has been reported. Phenyl rotation also involves an interplay between edge-to-face π−π, face-to-face π−π and metal coordination interactions that govern the formation and motion of the grid. Because of the relative simplicity of this motion, and the fact that it is amenable to study by ^{1}H NMR, study of this process provides an important insight into the interactions involved in self-assembly and dynamic motions of other self-assembled grid systems. Such understanding should also facilitate the design of new grid ligands for particular applications. We report our studies of the phenyl group rotation in these systems through the modification of ligand structure and variable temperature ^{1}H NMR.

Experimental

General

^{1}H NMR spectra were recorded at 300 or 400 MHz and referenced to internal solvent protons. Coupling constants are reported in Hertz. The temperature recorded by the variable temperature probe was calibrated with an ethylene glycol standard (*17*). 2-Iodo-4,6-dimethylpyrimidine was synthesised by the method of Vlàd and Horvath (*18*). Ligands **1**, **2**, **5**, **6** and their zinc grid complexes were synthesised as previously reported in the literature (*14*, *19*). Ligands **3**, **4**, **7** and **8** are new; syntheses and spectral details are provided below. Zinc grid complexes of **3**, **4**, **7** and **8** were formed and studied in acetonitrile solution as described below.

General procedure for ^{1}H NMR experiments with grid complexes

Equimolar amounts of ligand and zinc triflate (typically 0.05 mmol) were combined in 1 ml acetonitrile-d3. After ~5 min–6 h depending upon ligand, ^{1}H NMR indicated the formation of a grid complex through the appearance of doublets corresponding to inner and outer phenyl protons (ligands **1**–**2**, **5**–**8**) or broad resonances corresponding to exchanging inner and outer phenyl protons (ligands **3** and **4**). Grid formation was also confirmed by electrospray mass spectrometry. Variable temperature ^{1}H NMR was performed on this solution, and subsequently (for ligands **1**–**4**) aliquots (typically 0.5–1.0 μl) of triethylamine were added. After the addition of each aliquot, the variable temperature experiment was repeated. For those systems where the chemical shift of inner and outer resonances could be determined, rates of exchange between inner and outer protons were determined by simulation using either winDNMR (*20*) or SPINEVOLUTION (*21*). Optimisation of the fit was performed manually using winDNMR; SPINEVOLUTION includes optimisation code. Because there is a significant temperature dependence of the chemical shift on these protons, simulations optimised both chemical shift and rate constant to obtain the best fit to experimental spectra. Above the coalescence temperature, rate and chemical shift difference cannot be determined independently, providing an upper limit to the temperature of meaningful simulations. Spectral details for the zinc grid complexes of **3H$_2$** **4H$_2$**, **7** and **8** are provided below, full sets of spectra are provided as Supplementary Information, available online. Labels used for peak assignments are shown in Scheme 1.

$[(7)_4Zn_4]^{8+}(OTf^-)_8$

^{1}H NMR (acetonitrile-d3, −17°C) 8.13 (s, 4H, H^{pym}), 7.96 (s, 8H, H^{imine}), 7.85 (ddd, 8H, J = 8.4, 7.2, 1.5, H^4), 7.36 (dd, 8H, J = 5.3, 1.5, H^6), 7.31 (d, 8H, J = 8.4, H^3), 6.92 (dd, 8H, J = 5.3, 7.2, H^5), 6.75(dd, 4H, J = 8.5, 2, H^o), 6.70 (dd, 4H, J = 8, 2, H$^{o'}$), 5.74 (dd, 4H, J = 8.5, 2, H^m), 5,66 (dd, 4H, J = 8, 2, H$^{m'}$), 4.28 (s, 12H, CH_3O—), 3.49 (s, 24H, CH_3N); ES-MS m/z = 665 $\{([(\mathbf{7})_4Zn_4](OTf^-)_4\}^{4+}$.

$[(3)_4Zn_4]^{8+}(OTf^-)_8$

^{1}H NMR (acetonitrile-d3, 20°C) 8.15 (s, 4H, H^{pym}), 7.96 (s, 8H, H^{imine}), 7.75 (ddd, 8H, J = 8.5, 7, 1.5, H^4), 7.40 (dd, 8H, J = 4.5, H^6), 7.03 (d, 8H, J = 8.5, 7, H^3), 6.86 (dd, 8H, J = 5.3, 7.2, H^5), 6.8 (bs 8H, H°), 5.76 (bs, 8H, H^m), 4.30 (s, 12H, CH_3O—); ES-MS m/z = 1952 $\{[(\mathbf{3})_4Zn_4] - 7H\}^+$.

$[(8)_4Zn_4]^{8+}(OTf^-)_8$

^{1}H NMR (acetonitrile-d3) 8.12 (s, 4H, H^{pym}) 7.95 (s, 8H, H^{imine}), 7.84 (dd, 8H, J = 8.4, 8.8, H4), 7.35 (d, 8H, J = 5.3, H^6), 7.31 (d, 8H, J = 8.8, H^3), 6.93 (t, 8H, J = 5.3,8.4, H^5), 6.41 (d, 4H, J = 8.5, H°), 6.12 (d, 4H, J = 8.5, H$^{o'}$), 5.58 (d, 4H, J = 8.5, H^m), 5.40 (d, 4H, J = 8.5, H$^{m'}$), 3.50 (s, 24H, CH_3N), 3.40 (s, 24H, $(CH_3)_2N$—); ES-MS m/z = 678 $\{([(\mathbf{8})_4Zn_4](OTf^-)_4\}^{4+}$.

$[(4)_4Zn_4]^{8+}(OTf^-)_8$

^{1}H NMR (acetonitrile-d3) 8.05 (s, 4H, H^{pym}), 7.88 (s, 8H, H^{imine}), 7.72 (td, 8H, J = 8.4, 8.8, H^4), 7.37 (d, 8H, J = 4.4, H^6), 6.98 (d, 8H, J = 8.4, H^3), 6.83 (dd, 8H, J = 4.4, 8.4, H^5), 6.29 (bs, 8H, H°), 5.60 (d, 8H, J = 8.6, H^m), 3.39 (s, 24H, $(CH_3)_2NO$—); ES-MS m/z = 2002 $\{[(\mathbf{3})_4Zn_4] - 7H\}^+$, m/z = 1001 $\{[(\mathbf{3})_4Zn_4] - 6H\}^{2+}$.

Crystallography

Solvated crystals of $[(\mathbf{7})_4Zn_4]^{8+}(OTf^-)_8$ were grown by vapour diffusion of ether into an acetonitrile solution

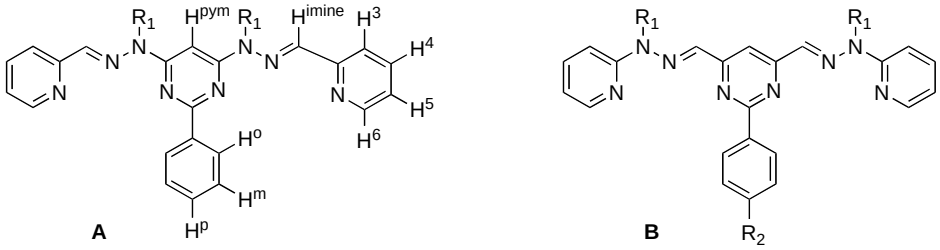

Label	Ligand Structure	R_1	R_2
1H$_2$	A	H	–
2H$_2$	B	H	H
3H$_2$	B	H	CH_3O
4H$_2$	B	H	$(CH_3)_2N$
5	A	CH_3	–
6	B	CH_3	H
7	B	CH_3	CH_3O
8	B	CH_3	$(CH_3)_2N$

Scheme 1. Ditopic hydrazone ligands used in this study.

containing equimolar amounts of **7** and $Zn(OTf)_2$. Examination of an orange block in the X-ray beam indicated a triclinic cell (space group $P-1$) with parameters $a = 14.820(2)$ Å, $b = 17.580(3)$ Å, $c = 30.895(5)$ Å, $\alpha = 86.730(2)$ Å, $\beta = 81.446(2)$ Å, $\gamma = 70.973(2)$ Å, $V = 7524.52$Å^3 and $Z = 2$. Intensities of 18,320 unique reflections were measured at 100 K. The structure was initially solved by direct methods. Refinement of the structure was complicated by extensive disorder amongst both the counterions and solvate molecules with additional disorder in the complex arising from the orientation of the methoxy groups with respect to the remainder of the ligand. Use of the SQUEEZE procedure (as implemented in the program PLATON (*22*)) to model the disordered solvent and counterions allowed for satisfactory refinement of the grid structure giving $R_1 = 7.65\%$, $wR_2 = 22\%$; GOF = 0.924.

Solvated crystals of $[(Zn^{2+})_4(\mathbf{2}^{2-})_4]$ were grown as golden pyramids from the evaporation of a THF solution containing $Zn(OTf)_2$, **2H$_2$** and excess Et_3N. Examination of a crystal in the X-ray beam indicated a tetragonal cell (space group $I4/a$) with parameters $a = 29.182(3)$ Å, $c = 13.4810(3)$ Å, $V = 11{,}480.2$ Å^3 and $Z = 8$. Intensities of 2578 unique reflections were measured at 100 K. Initial structure solution was by direct methods. Again, refinement was complicated by extensive regions of disordered solvent. Refining using SQUEEZE gave $R_1 = 5.38\%$, $wR_2 = 13.9\%$; GOF = 0.888.

Full details of both crystal structure determinations have been deposited with the Cambridge Crystallographic Database – deposition numbers 768,348 and 768,349.

4-Dimethylaminophenylboronic acid ethylene glycol ester (9)

Magnesium (2.4 g, 0.1 mol) was stirred in 100 ml THF, and a solution of *p*-bromo-*N*,*N*-dimethylaniline (20 g, 0.1 mol) in THF (200 ml) was added dropwise under a nitrogen atmosphere. After addition was complete, the mixture was heated under reflux until the magnesium had completely dissolved. The solution of the Grignard reagent was cooled to −78°C, and triisopropyl borate (18.8 g, 0.1 mol) was added dropwise. The resulting solution was allowed to warm to room temperature and hydrolysed by pouring into 100 ml 5 M hydrochloric acid. The solution was made basic (pH 13) with 10% NaOH solution and extracted with diethyl ether. The aqueous mixture was then re-acidified to pH 8 with 5 M hydrochloric acid, extracted with diethyl ether and the ether extract was dried and evaporated to give 8 g (50%) of the crude boronic acid as a white solid. Because this crude material was difficult to characterise, the ethylene glycol ester was prepared by dissolution in toluene, addition of 0.1 mol ethylene glycol and heating the resulting heterogenous mixture at 90°C for 1 h. After

cooling and removal of the ethylene glycol layer with a separatory funnel, evaporation of the toluene gave white plates that were recrystallised from toluene. m.p. 153–155°C ^{1}H NMR ($CDCl_3$) 3.00 (s, 6H), 4.33 (s, 4H) 6.67 (d, 2H, $J = 8.8$) 7.69 (d, 2H, $J = 8.8$); ^{13}C NMR ($CDCl_3$) 40.14, 65.89, 111.35, 129.19, 136.32, 152.68; IR (NaCl plate) 2900 (C—H), 1600 (aromatic C═C); EI-MS 191(M + , 72), 190 (100), 189 (23).

2-(4′-Dimethylaminophenyl)-4,6-dimethylpyrimidine (10)

To a solution of 764 mg (4 mmol) of 4-dimethylaminophenylboronic acid ethylene glycol ester and 936 mg (4 mmol) 4,6-dimethyl-2-iodopyrimidine in 20 ml dioxane were added 0.1 g of PPh_3 (0.4 mmol), 0.02 g of $Pd(OAc)_2$ (0.1 mmol) and 8 ml 1 M aqueous NaOH. The reaction mixture was degassed and heated at 70–80°C for 3 h. The cooled mixture was extracted with 3 × 100 ml portions of ethyl acetate. Organic extracts were combined and back extracted with 3 × 100 ml portions of 0.5 N HCl. The aqueous layer was neutralised with 1 N NaOH solution to pH 6 where the product precipitated as a cream solid and was isolated by filtration. Recrystallisation from heptane gave white needles (0.75 g, 80%) with m.p. 158–160°C; ^{1}H NMR ($CDCl_3$) δ 2.48 (s, 6H), 3.03 (s, 6H), 6.75 (d, 2H, $J = 9$), 6.78 (s, 1H), 8.33 (d, 2H, $J = 9$); ^{13}C NMR ($CDCl_3$) δ 24.3, 40.3, 111.7, 116.4, 126.0, 129.4, 152.0, 164.5, 166.4; IR (NaCl plate) 2920 (C—H), 1606 (aromatic C═C); EI-MS 227 (M+, 100), 226 (90), 211 (11), 145 (11).

2-(4′-Dimethylaminophenyl)-pyrimidine-4,6-dicarboxaldehyde (12)

To a solution of 2-(4′-dimethylaminophenyl)-4,6-dimethylpyrimidine (0.68 g, 3 mmol) in dioxane (20 ml) were added SeO_2 (6.2 mmol) and trifluoroacetic acid (7 ml). The solution was heated under reflux for 2 h, then filtered and neutralised with saturated $NaHCO_3$ solution. The mixture was then extracted with dichloromethane, and the organic extract was filtered through a plug of silica gel. Evaporation gave an orange solid containing the dicarboxaldehyde, 131 mg, 0.51 mmol (17%) ^{1}H NMR ($CDCl_3$) 3.03 (s, 6H), 6.75 (d, 2H, $J = 9$ Hz), 7.86 (s, 1H), 8.41 (d, 2H $J = 9$ Hz), 10.05 (s, 2H); ^{13}C NMR ($CDCl_3$) 40.3, 107.9, 111.8, 130.2, 130.3, 152.8, 160.2, 16.1, 192.8; IR (NaCl plate) 2920, 2846 (C—H), 1719 (C═O), 1606 (aromatic C═C); EI-MS 255 (M + , 100), 254 (80) 198 (15), 145 (30). This solid was not purified further but used directly in the next step.

2-(4′-Dimethylaminophenyl)-pyrimidine-4,6-dicarboxaldehyde bis(2-pyridyl hydrazone) (4H$_2$)

Crude 2-(4′-dimethylaminophenyl)-pyrimidine-4,6-dicarboxaldehyde (130 mg, 0.5 mmol) was redissolved in ethanol (40 ml), and 6 mmol 2-hydrazinopyridine in ethanol was added. Slow evaporation of the ethanol precipitated the bishydrazone as an orange solid (220 mg, 98%) with ^{1}H NMR (dmso-d6) 11.53 (s, 2H), 8.25 (d, 2H, $J = 9.1$), 8.19 (ddd, 2H, $J = 4.9$, 1.8, 0.8), 8.05 (s, 2H), 7.99 (s, 1H), 7.76 (ddd, 2H, $J = 8.2$, 7.2, 1.8), 7.39 (dt, 2H, $J = 8.2$, 0.8), 6.89 (ddd, 2H, $J = 7.2$, 4.9, 0.8), 6.8 (d, 2H, $J = 9.06$), 3.31 (s, 6H); ^{13}C NMR (dmso-d6) 164.1, 160.1, 156.2, 152.0, 147.9, 138.4, 137.6, 129.0, 124.2, 116.3, 111.4, 106.9, 105.2. HETCOR indicates that the N-methyl carbons are near 40 ppm and lost under the solvent peak; IR (NaCl plate) 3203(C—H), 1606 (aromatic C═C); HRMS 438.2156 (M + H, calcd 438.2155) 460.1973 (M + Na, calcd 460.1974).

2-(4′-Dimethylaminophenyl)-pyrimidine-4,6-dicarboxaldehyde bis(2-pyridyl methyl hydrazone) (8)

2-(4′-Dimethylaminophenyl)-pyrimidine-4,6-dicarboxaldehyde bis(2-pyridyl hydrazone) (18 mg) was combined with excess NaH in THF and excess MeI and stirred until the purple colour was entirely dissipated. Dilution with water, extraction with dichloromethane, evaporation and recrystallisation gave the dimethyl hydrazone (13 mg, 70%) ^{1}H NMR (dmso-d6) 8.33 (d, 2H $J = 8.8$ Hz), 8.30 (2H dd, $J = 5$, 2 Hz), 8.14 (s, 1H), 7.78 (d, 2H, $J = 8.5$), 7.65 (s, 2H), 7.58 (2H, ddd, $J = 2$, 7, 8.5), 6.81(2H, dd, $J = 5$, 7), 7.72 (d, 2H, $J = 8.8$), 3.67 (s, 6H), 2.99 (s, 6H); ^{13}C NMR (dmso-d6) 165.1, 161.8, 157.2, 152.1, 147.1,137.5, 133.5, 129.4, 116.7, 111.7, 110.3, 106.3, 40.3, 29.9; IR 1604 (aromatic C═C); HRMS 466.2468 (M + H, calcd 466.2467).

*2-(*p*-Methoxyphenyl)-4,6-dimethylpyrimidine (11)*

To a solution of 8 mmol (1.22 g) of *p*-methoxyphenylboronic acid and 8 mmol (1.87 g) 2-iodo-4,6-dimethylpyrimidine in 50 ml dioxane were added 0.1 g of PPh_3 (0.4 mmol), 0.02 g of $Pd(OAc)_2$ (0.1 mmol) and 15 ml aq 1 M NaOH solution. The reaction mixture was heated under nitrogen at 70–80°C for 3 h. Then the cooled mixture was diluted with ethyl acetate and extracted with 0.5 N HCl. The aqueous layer was neutralised with 1 N NaOH solution whereupon the solution turned cloudy and upon standing a crystalline precipitate of the product was isolated by filtration. The crude product was purified by recrystallisation from heptane to give 0.9 g (4.2 mmol, 53%) of white crystals with m.p. 95–96°C ^{1}H NMR ($CDCl_3$) δ 2.509 (s, 6H), 3.88 (s, 3H), 6.97 (s, 1H), 6.861 (d, 2H, $J = 9$), 8.387 (d, 2H, $J = 9$); ^{13}C NMR ($CDCl_3$) δ 24.2, 55.4, 113.8, 117.3, 129.9, 131.1, 161.6, 163.9, 166.6; MS *m/z* 214 (M + , 100), 199 (30), 171 (10), 133 (15); IR (NaCl plate) 2997, 2970, 2935, 2835, (C—H), 1591 (C═C).

*2-(*p*-Methoxyphenyl)-pyrimidine-4,6-dicarbaldehyde (13)*

2-(*p*-methoxyphenyl)-4,6-dimethylpyrimidine (0.42 g, 2 mmol) was dissolved in 20 ml of dioxane. To this was added the solution of 1.10 g of SeO_2 (2.2 mmol) in 1 ml of water and 5 ml trifluoroacetic acid. The reaction mixture was refluxed for 2 h. The resulting brown solution was filtered, neutralised with saturated aqueous $NaHCO_3$ and extracted with dichloromethane. The dichloromethane extract was filtered through silica gel and evaporated to leave a yellow solid containing largely the dialdehyde (0.1 g. 20%) with ^{1}H NMR ($CDCl_3$) 3.92 (s, 3H), 7.06 (d, 2H, $J = 8.8$), 8.58 (d, 2H, $J = 8.8$), 8.05 (s, 1H), 10.16 (s, 2H); ^{13}C NMR ($CDCl_3$) 55.5, 109.1, 114.3, 128.2, 130.5, 160.2, 163.0, 166.6, 192.4; MS(EI) *m/z* 242 (M + ,100), 185 (50), 158 (40); IR (NaCl plate) 3060, 2973, 2933, 2844 (C—H), 1714 (C═O), 1606 (C═C). The aldehyde was not purified further but used directly in the next step.

*2-(*p*-Methoxyphenyl)-pyrimidine-4,6-dicarbaldehyde bis(2-pyridyl hydrazone) ($3H_2$)*

To a solution of 0.24 g (1 mmol) of crude 2-(*p*-methoxyphenyl)-pyrimidine-4,6-dicarbaldehyde (1 mmol) in ethanol was added solution of excess (0.44 g) of 2-hydrazinopyridine in ethanol. The solution was stirred for 1 h. The yellow precipitate was recrystallised from tetrahydrofuran/heptane to give 0.48 g (100%) of a cream coloured residue. ^{1}H NMR (dmso-d6) 3.85 (s, 3H, CH_3O—), 6.91 (dd, 2H, $J = 5.0$, 7.0, H^5), 7.09 (d, 2H, $J = 9.1$, H^m), 7.42 (d, 2H, $J = 8.25$, H^3), 7.78 (ddd, 2H, $J = 8.2$, 7.0, 1.3, H^4), 8.08 (s, 2H, H^{imine}), 8.09 (s, 1H, H^{pym}), 8.21 (dd, 2H, $J = 5.0$, 1.3, H^6), 8.38 (d, 2H, $J = 9.1$, H°), 11.61 (s, 2H, NH); ^{13}C NMR (dmso-d6) 55.9, 106.8, 107.6, 114.6, 117.0, 130.0, 139.0, 139.7, 148.6, 156.8, 161.8, 162.1, 164.0, 171.2; IR (NaCl plate) 3206, 2964, 2921, 2852 (C—H), 1608 (C═C); HRMS 425.1829 (MH+, calcd 425.1838).

*2-(*p*-Methoxyphenyl)-pyrimidine-4,6-dicarbaldehyde bis(2-pyridyl methyl hydrazone) (7)*

2-(*p*-Methoxyphenyl)-pyrimidine-4,6-dicarbaldehyde bis(pyridine-2-hydrazone) (52 mg, 0.12 mmol) was combined with excess NaH in 10 ml THF to form a dark blue-purple solution. Excess iodomethane (0.5 ml) was added, and the solution was stirred until the purple colour was entirely dissipated. The mixture was diluted with water, and the precipitated solid was removed by filtration. The solid was recrystallised by the evaporation of dichloromethane from a solution in dichloromethane/heptane to give 16 mg of product (30%) with ^{1}H NMR($CDCl_3$) 8.48 (d, 2H, $J = 9$ Hz, H°), 8.3 (m, 3H, H^{pym}, $H^{6'}$), 7.87 (d, 2H, $J = 8.7$ Hz, $H^{3'}$), 7.75 (s, 2H, H^{imine}), 7.67 (td, 2H, $J = 2$, 8, $H^{4'}$), 7.03 (d, 2H, $J = 9$ Hz, H^m), 6.91(dd, 2H, $J = 5.8$, 6.3 $H^{5'}$), 3.90 (s, 3H, CH_3O—), 3.77 (s, 6H, CH_3N); ^{13}C NMR ($CDCl_3$) 162.0, 157.1, 147.1, 137.6, 133.0, 129.8, 116.9, 113.9, 110.4, 55.4, 30.0; IR (NaCl plate) 2916, 2849 (C—H) 1655 (C═N); HRMS 453.2137 (M + H, calcd 453.2151), 457.1962 (M + Na, calcd 457.1971).

Results

Ligand synthesis

Eight different ditopic hydrazone ligands were studied, of which four are new. Structures are shown in Scheme 1 along with the labels for protons in the ^{1}H NMR.

Phenyl-substituted ligands **$1H_2$**–**$2H_2$** and **5**–**6** were synthesised as reported previously (*14*). 4-Methoxy and 4-dimethylamino-substituted ligands (**$3H_2$** and **$4H_2$**) were synthesised through Suzuki coupling of the corresponding boronic acid or boronate ester with 4,6-dimethyl-2-iodopyridine. Oxidation of the resulting pyrimidine with selenium dioxide gave the desired dialdehyde in relatively low yield, though the reaction rate was significantly enhanced by the addition of trifluoroacetic acid. Reaction of the dialdehyde with 2-hydrazinopyridine gave the desired ligands as yellow or orange solids. Ligands methylated on the hydrazone nitrogen (**7**–**8**) were obtained by deprotonation of **$3H_2$**–**$4H_2$** with NaH or KOtBu in THF and alkylation with excess methyl iodide as previously reported for **6** (*14*) (Scheme 2).

Crystallography

Single crystals of two complexes $[Zn_4(\mathbf{7})_4]^{8+}(OTf^-)_8$ and $Zn_4(\mathbf{2}^{2-})_4$ were studied by X-ray crystallography. Thermal ellipsoid plots of both structures are shown in Figure 1. $Zn_4(\mathbf{7})_4]^{8+}(OTf^-)_8$ crystallises in the triclinic space group $P-1$ with two grid complexes per unit cell. The four independent ligands composing the grid show similar geometry, with the phenyl ring perpendicular to the rest of the ligand and intercalated between the neighbouring ligands. The methoxy group lies in the plane of the phenyl ring, though there is some orientational disorder with the methyl pointing either towards or away from the centre of the grid. Though most of the triflate anions could be located they, along with the solvate, show considerable disorder.

$Zn_4(\mathbf{2}^{2-})_4$ crystallises in the tetragonal space group I_4/a. The grid complex lies on an $\mathbf{S_4}$ axis with the four metal ions and ligands of the grid related by symmetry. As with similar grid complexes, the phenyl rings are perpendicular to the attached ligand and intercalated between neighbouring ligands. Though there is no disorder in the grid itself, the remainder of the unit cell is occupied by extensively disordered solvent molecules.

Both structures are typical for such grid complexes and show intercalated phenyl rings with relatively short π–π

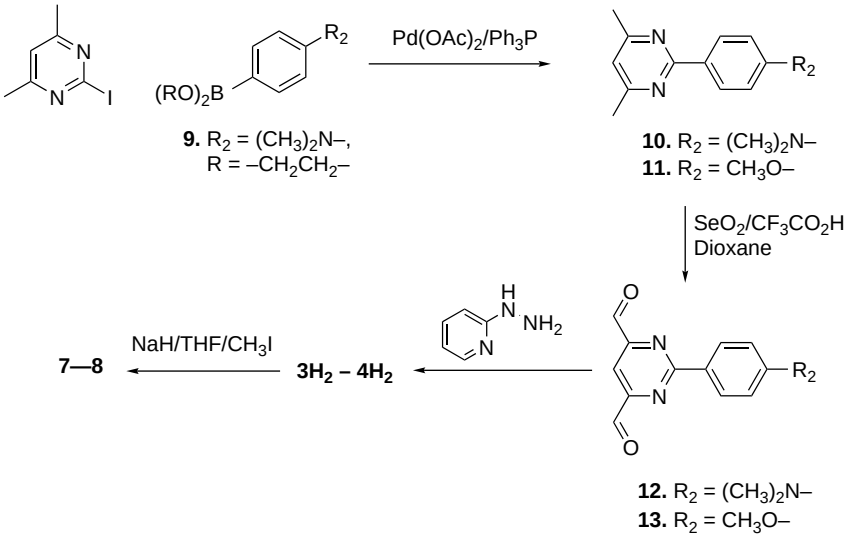

Scheme 2. Synthesis of ligands **3**–**4** and **7**–**8**.

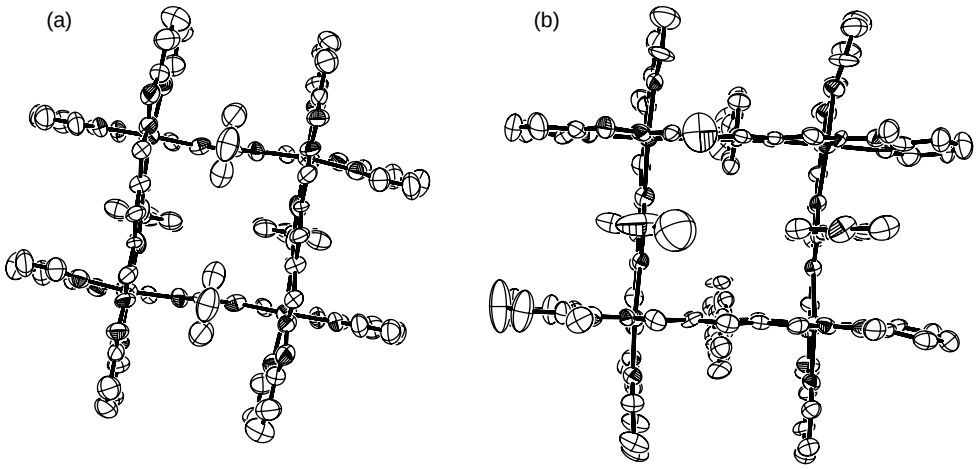

Figure 1. Thermal ellipsoid plots for (a) $Zn_4(\mathbf{2}^{2-})_4$ and (b) $Zn_4(\mathbf{7})_4(OTf)_8$. Counterions and disordered solvent molecules are not shown.

stacking distances. Averages of Zn–ligand bond lengths for these and related compounds are listed in Table 1 along with approximate π-stacking distances. Full details of data acquisition and refinement are given in the supplementary material.

^{1}H NMR

In general, grids were formed *in situ* from equimolar amounts of ligand and $Zn(OTf)_2$ in acetonitrile or deuterated acetonitrile. ^{1}H NMR spectra of the grid complexes at 25°C showed either inner and outer phenyl

Table 1. Average metal–ligand distances and phenyl–ligand π-stacking distances (Å) for $Zn_4(\mathbf{7})_4(OTf)_8$, $Zn_4(\mathbf{2})_4$ and related species.

Grid complex	Zn–N^{pym}	Zn–N^{hyd}	Zn–N^{py}	Phenyl–Ligand[a]
$Zn_4(\mathbf{2}^{2-})_4$	2.24(5)[b]	2.106(2)[b]	2.166(4)[b]	3.283
$Zn_4(\mathbf{7})_4(OTf)_8$	2.23(1)[c]	2.13(1)[c]	2.14(2)[c]	3.30
$Zn_4(\mathbf{5})$	2.213(7)[c,d]	2.140(4)[c,d]	2.17(1)[c,d]	3.25[d]

Note: Values in parentheses are standard deviations based on the values averaged.
[a] Distance from the centroid of phenyl ring to plane defined by the hydrazone N—N—C unit.
[b] Average of two independent values.
[c] Average of eight independent values.
[d] Data from Ref. (*14*).

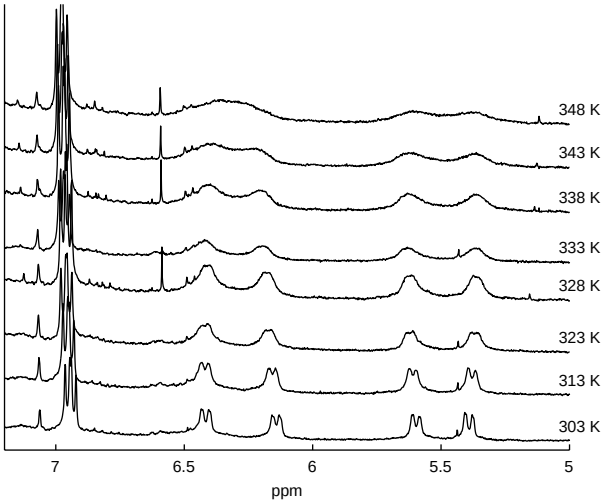

Figure 2. VT ^{1}H NMR spectra of *ortho*- and *meta*-phenyl protons of grid formed from ligand **8** and Zn^{2+} in acetonitrile.

resonances consistent with phenyl intercalation (Figure 2) or broadened resonances consistent with the rotation of the phenyl group in a restricted environment (Figure 3).

Further information was obtained by recording spectra at a range of temperatures and, for the ligands with free NH groups, a range of amounts of added triethylamine (Figures 2 and 3, Supplementary Information, available online). As previously noted with $[Zn_4(\mathbf{2H_2})_4]^{8+}$ (*14*), in the initial stages of titration, triethylamine quantitatively deprotonates the acidic hydrazone hydrogens. In the ^{1}H NMR of the grid complex, the pyrimidine proton undergoes an upfield shift directly proportional to the amount of added base. Because the total amount of base in the sample includes impurities such as water, we estimated

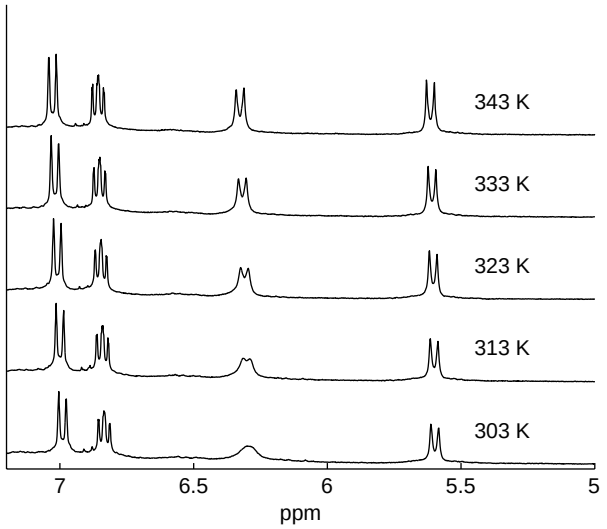

Figure 3. VT ^{1}H NMR spectra of *ortho*- and *meta*-phenyl protons of grid formed from ligand $\mathbf{4H_2}$ and Zn^{2+} in acetonitrile.

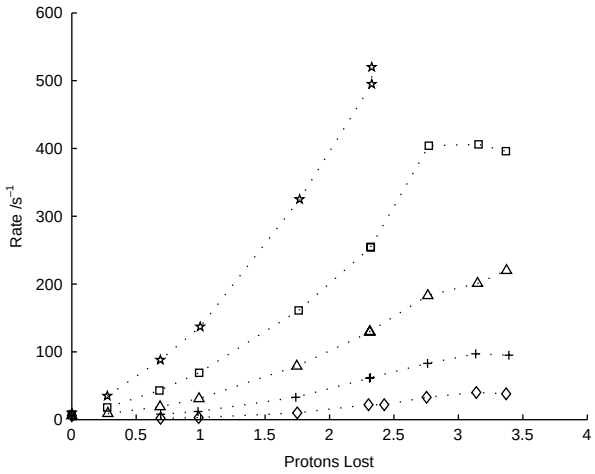

Figure 4. Rate of phenyl rotation vs. NH protons lost from $[Zn_4(\mathbf{1H_n})_4]^{4n+}$ at 296 K (diamonds), 306 K (crosses) 316 K (triangles), 326 K (squares) and 335 K (stars). The average number of protons lost was determined indirectly through the chemical shift of the pyrimidine proton. At high temperatures and levels of deprotonation, extreme linebroadening prevented the accurate determination of rate.

the degree of deprotonation of the ligand using the pyrimidine proton chemical shift with a sample containing a crystal of toluene sulfonic acid as the 'zero' point. While the complex from ligand **5** shows little spectral change with temperature, that from $\mathbf{1H_2}$ shows broadening of the phenyl resonances as a result of both increased temperature and increased base concentration (Supplementary Information, available online). Simulation of the lineshape gave rate constants plotted in Figure 4. Rates were fitted to the Arrhenius equation to obtain activation energies and pre-exponential factors plotted as a function of deprotonation in Figure 5. Beyond a 1:1 base to ligand

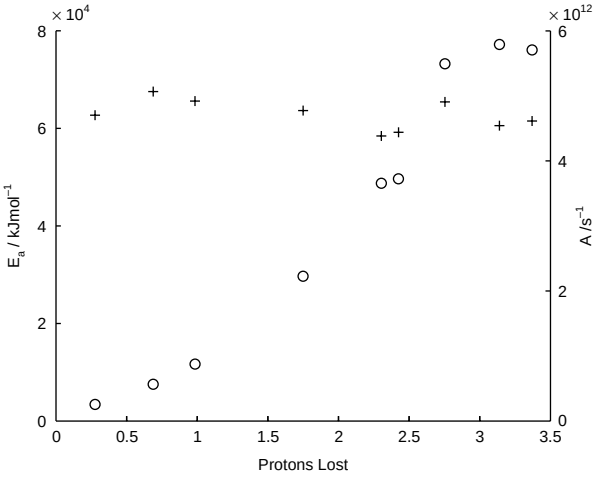

Figure 5. Dependence of Arrhenius parameters for phenyl rotation, E_a (crosses) and A (circles) on protons lost from $[Zn_4(\mathbf{1H_n})_4]^{4n+}$.

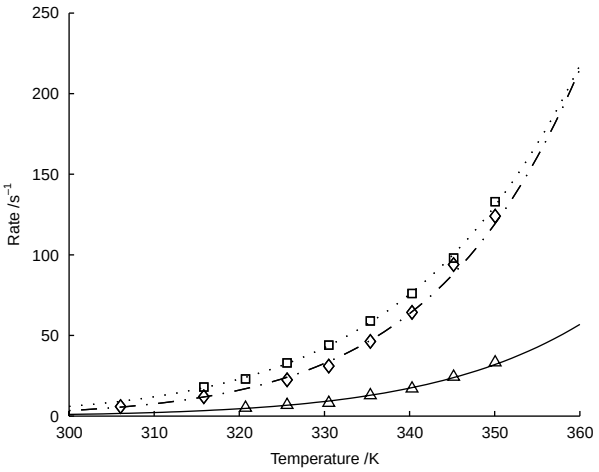

Figure 6. Rate of phenyl rotation vs. temperature for $[Zn_4(\mathbf{6})_4]^{8+}$ (triangles), $[Zn_4(\mathbf{7})_4]^{8+}$ (squares) and $[Zn_4(\mathbf{8})_4]^{8+}$ (diamonds). Lines are best fits to the Arrhenius equation.

ratio, the experiment was complicated by precipitation of a partly deprotonated grid and was not continued.

The grid complex from ligands **2** and **6** shows similar behaviour, though the chemical shift difference between inner and outer protons is much smaller. For **6**, broadening of the resonances as a result of phenyl rotation is observed, but for $\mathbf{2H_2}$, even small amounts of base reduce the coalescence temperature for the phenyl resonances such that distinct inner and outer resonances are not observed. The substituted ligands $\mathbf{3H_2}$–$\mathbf{4H_2}$ and **7**–**8** also form grids. For the methylated ligands inner and outer resonances can be observed; however, for the protonated ligands we found no conditions allowing for the observation of inner and outer phenyl resonances. Instead peaks are observed that broaden or narrow as a function of temperature and base concentration (Figure 3). Simulation of spectra gave rates for phenyl rotation for the methylated grids plotted as a function of temperature in Figure 6. Arrhenius parameters are presented in Table 2. Full sets of VT ^{1}H NMR spectra are presented in the Supplementary Information, available online.

Table 2. Activation energies and Arrhenius constants for phenyl rotation in grid complexes.

Grid	E_a (kJ/mol)	A ($\times 10^{11}$ s^{-1})
$[Zn_4(\mathbf{1H_n})_4]^{4n+}$	63(3)[a]	2.5–57[b]
$[Zn_4(\mathbf{6})_4]^{8+}$	60(1)	0.34
$[Zn_4(\mathbf{7})_4]^{8+}$	54(3)	0.14
$[Zn_4(\mathbf{8})_4]^{8+}$	62(2)	2.2

Note: [a]Average value and standard deviation determined from nine different levels of deprotonation, *n*.
[b]Dependent on level of deprotonation *n*; see Figure 5.

Discussion

Though many grid complexes have been described (*12*, *23*), rotation of an intercalated phenyl group has only previously been noted upon deprotonation of the hydrazone grids from ligand $\mathbf{2H_2}$. The current data suggest that phenyl group rotation, at least in the hydrazone series of complexes, is far more common. The only complex where no evidence of phenyl group rotation was observed was the case of ligand **5**.

It should be noted, however, that observation of exchange between sites is dependent upon the frequency difference between the exchanging resonances; these dynamic effects may not have been previously noted because ^{1}H NMR spectra were recorded on higher field instruments.

In all the grid complexes with intercalated phenyl groups studied by crystallography so far, the phenyl group is tightly packed between two neighbouring ligands. The phenyl–ligand distance is on the order of typical π-stacking interactions (~3.3 Å), and the current grids are no exception to this. Considering this geometry, it is unlikely that the phenyl group can rotate without partial dissociation of a neighbouring ligand or ligands. Three simple scenarios are illustrated in Figure 7.

i) Rate limiting dissociation of one or more coordinated atoms allows the phenyl group to rotate freely until re-association of the ligand (Figure 7(a), $k_1 << k_2$).
ii) Equilibrium dissociation of one or more coordinated atoms is followed by rate limiting rotation of the phenyl ring in a restricted environment (Figure 7(a), $k_1 >> k_2$).
iii) Rotation of the phenyl ligand accompanies (or forces) dissociation of coordinated atoms in a concerted manner (Figure 7(b)).

We can make a further distinction between dissociation of the terminal pyridine ligand (the mechanism originally suggested) and dissociation of the central pyrimidine. Based on tabulated pK_a data, pyrimidine is significantly less basic than pyridine (pK_a(pyridinium) = 5.30, pK_a(-pyrimidinium) = 1.23) suggesting that the latter is more likely. This is born out by our data (*vide infra*).

Further insight comes from temperature and base dependence of phenyl rotation on the $[Zn_4(\mathbf{1H_n})_4]^{4n+}$ series of grids. In this system, rotation of the phenyl group can occur at varying levels of deprotonation; thus, the system has multiple reaction pathways that are degenerated in that they produce the same effect (rotation of the phenyl ring), but may have different rate constants. The overall (measured) rate constant will be the sum of contributions from all possible pathways, i.e.

$$k_{obs} = k_0x_0 + k_1x_1 + k_2x_2 + \ldots + k_8x_8,$$

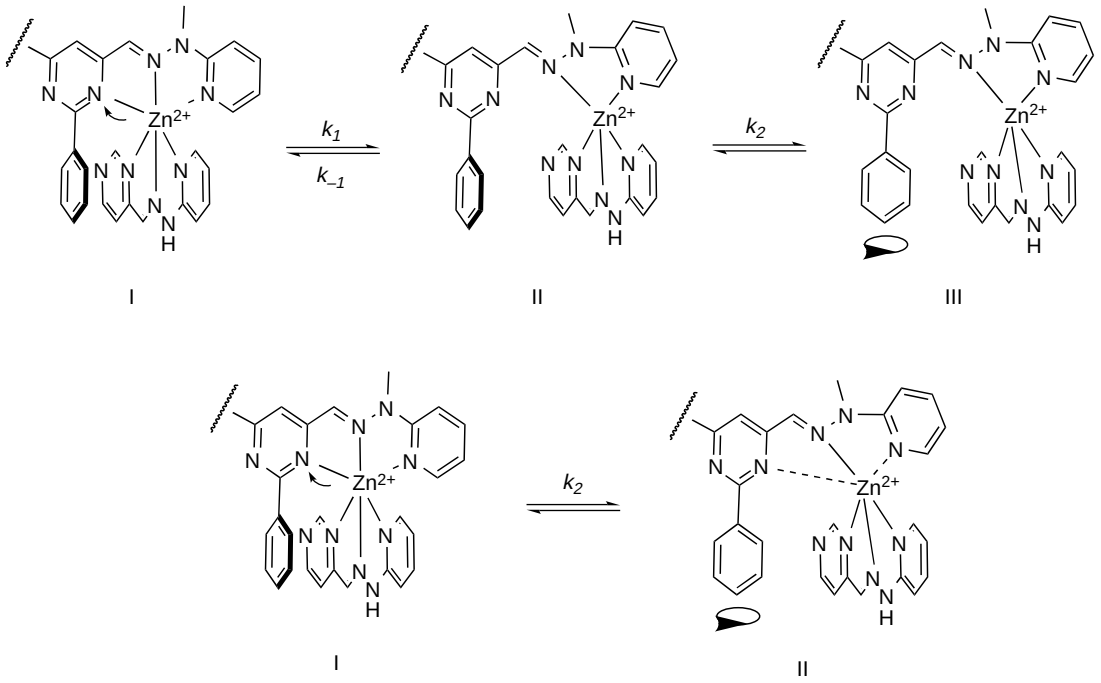

Figure 7. (a) Stepwise and (b) concerted mechanisms for phenyl ring rotation (dissociation at the pyrimidine is shown, only one metal centre is shown for clarity). Two possibilities exist for the stepwise mechanism depending upon whether ligand dissociation (mechanism i) or phenyl rotation (mechanism ii) is rate determining.

where k_n and x_n are, respectively, the rate constant and mole fraction of the grid complex having lost n NH protons. Surprisingly, despite the complex nature of the system, activation energies determined using the observed rate k_{obs} indicate that the activation energy for phenyl rotation was essentially independent of deprotonation of the ligand, and the variation in rate was largely determined by the pre-exponential factor A. These values are shown in Figure 5. These data are consistent with a model where only a fraction of the molecules is capable of undergoing phenyl rotation at any one time and that this fraction, incorporated into the pre-exponential factor A, is relatively independent of temperature. The fraction capable of rotation may be influenced by deprotonation of the ligand, but this cannot be the sole contributing factor since rotation also occurs with the methylated ligands. In fact, the activation energies for the methylated ligands were similar to the (partly) deprotonated system (Table 2), suggesting that deprotonation does *not* significantly influence the transition state for phenyl rotation.

The data are overall consistent with mechanism (ii) in Figure 7 provided that the dissociation/association pre-equilibrium is fast on the ^{1}H NMR timescale, and $\Delta H_{eq} \approx 0$. Under these circumstances, ^{1}H NMR sees the average spectrum of dissociated and undissociated ligands, but only the latter can undergo phenyl rotation, and thus, the measured rate of phenyl rotation increases with increasing dissociation. Furthermore, with $\Delta H_{eq} \approx 0$ the equilibrium constant, $K = k_1/k_{-1}$, will be weakly temperature dependent, and thus, the temperature dependence on the rate is dominated by the activation energy of the phenyl rotation. Given that $\Delta H_{eq} \approx 0$, this further implies that in a solution at room temperature, there is substantial dissociation of the pyrimidine ring from the metal centre. The extent of this dissociation is related to the magnitude of the pre-exponential factor A.

With a basic mechanistic framework in place, the variations in pre-exponential factor and activation energy can be examined in more detail. The biggest variations in A are related to the deprotonation of the ligand NH groups in the $[Zn_4(\mathbf{1H_n})_4]^{4n+}$ series. As noted for iron hydrazone complexes, deprotonation of coordinated hydrazones increases electron density at the metal ion (*13*). The resulting reduced acidity of the metal allows the most weakly coordinated ligand (in this case the pyrimidine) to dissociate, and thus, allows for rotation of the phenyl group. Such base-dependent dissociations are well established in coordination chemistry. Dissociation probably also increases as a result of repulsion between electron-rich hydrazonide anions and the intercalated phenyl ring. For $[Zn_4(\mathbf{1H_n})_4]^{4n+}$, the dependence of A upon the degree of deprotonation is greater than first order (Figure 5). This suggests that phenyl rotation probably occurs via a multiple deprotonated species and further, that at least two ligand dissociations are required for the rotation to proceed. It is interesting to note that A appears

to reach a maximum value near the point where three protons are lost; this could have two possible interpretations: either at this level of deprotonation, all of the pyrimidine rings are completely dissociated, or that further deprotonation does not result in any significant increase in dissociation (possibly a result of increased strain in the partly dissociated system). At the opposite end of the scale, in the fully methylated grid $[Zn_4(\mathbf{5})_4]^{8+}$, no phenyl rotation, and by inference, no dissociation, is observed. In fact, this particular grid (but none of the others) is rigid enough to show a violet fluorescence (*19*). This further implies that any phenyl rotation in $[Zn_4(\mathbf{1H_n})_4]^{4n+}$ is due to the deprotonation resulting from low concentrations of basic impurities (such as water or excess ligand) in the solution.

When the ligand structure is changed to place the hydrazone nitrogens on the outside of the ligand (grids $[Zn_4(\mathbf{2H_n})_4]^{4n+}$ and $[Zn_4(\mathbf{6})_4]^{8+}$), phenyl rotation is observed under all circumstances. For the grid $[Zn_4(\mathbf{2H_n})_4]^{4n+}$, even with a small fraction of the ligands deprotonated, the coalescence point of the phenyl resonances is below the useful temperature range of the solvent in the 300 MHz ^{1}H NMR. This is probably largely due to the small difference in chemical shift between inner and outer phenyl protons. As previously noted, the activation energy for $[Zn_4(\mathbf{6})_4]^{8+}$ is within experimental error of the value for $[Zn_4(\mathbf{5})_4]^{8+}$. The difference in rate is again born by the pre-exponential factor (Table 2), suggesting that the same mechanistic considerations apply. Examination of the ligand structure suggests that in the ligands $\mathbf{2H_2}$ and **6**, the pyrimidine ring, substituted by two electron-withdrawing imine carbons rather than electron-donating amine nitrogens, is significantly less basic and thus dissociates more readily. This seemingly minor change allows for pyrimidine dissociation even without the assistance of an anionic ligand.

For the methoxy- and dimethylamino-substituted grids $[Zn_4(\mathbf{3H_2})_4]^{8+}$ and $[Zn_4(\mathbf{4H_2})_4]^{8+}$, the rate of phenyl rotation is fast enough that no inner and outer phenyl protons are observed, even without the addition of base. We cannot determine absolute rates because the inner and outer chemical shifts are not known, so interpretation of this observation must be somewhat speculative. We can, however, list some possible contributing factors. The most mundane would be that a small chemical shift difference between inner and outer resonances makes the exchange process more visible; however, this seems unlikely considering the methyl analogues. Other contributors may be electronic effects resulting from the substituent (vide supra), but also the substituent may act as an internal base to deprotonate the hydrazone and facilitate dissociation/phenyl rotation (Figure 8). This is supported by the models based on the known crystal structures that give a distance of $\sim$4 Å between the *para*-substituent and the hydrazone NH proton.

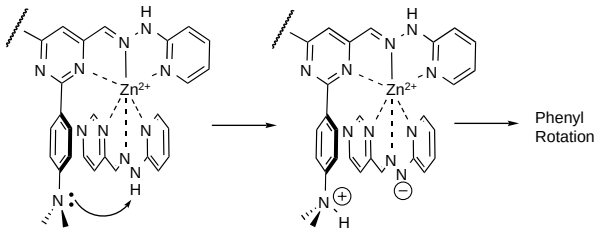

Figure 8. Possible role of proton transfer in phenyl rotation of grids from ligands $\mathbf{3H_2}$ and $\mathbf{4H_2}$.

As in the previous systems, methylation of the ligand prevents proton transfer and slows phenyl rotation. Comparison of the temperature dependence of the three systems based on ligands **6**, **7** and **8** (Table 2) shows that there is an additional dependence of the dissociation resulting from substituents on the phenyl ring. Since these substituents cannot effect the steric interactions in phenyl rotation, the effect is most probably electronic in origin. The pre-exponential factor A (and thus presumably the level of ligand dissociation in solution) decreases in the order $\mathbf{8} > \mathbf{6} > \mathbf{7}$ (i.e. $(CH_3)_2N$—, H—, CH_3O—). This follows the Hammett σ_m parameter for the substituents of which the corresponding values are -0.15, 0.0 and $+0.10$. The ligand HOMO, which is located largely on the N and C of the hydrazone, overlaps in a π-stack with the phenyl ring at the *meta*-position relative to the substituent. When this position is electron rich (ligand **8**), repulsion between the π systems in the stacked arrangement is increased, facilitating dissociation. Conversely, the methoxy substituent is electron withdrawing at this position, and the favourable interaction between π systems tends to reduce dissociation. It is interesting to compare this with the dimethylaminophenyl/polypyridyl system reported by Lehn 10 years ago. That system shows restricted rotation of the dimethylamino group but not the phenyl group (*11*). Furthermore, a strong visible absorption ascribed to a phenyl–pyridyl charge transfer transition was observed ($\lambda_{max} = 516$ nm). By comparison, the longest wavelength absorption for both $[Zn_4(\mathbf{8})_4]^{8+}$ and $[Zn_4(\mathbf{7})_4]^{8+}$ has $\lambda_{max} = 462$ nm. These observations illustrate the change in $\pi-\pi$ interaction upon substitution of an electron-deficient pyridyl group with an electron-rich hydrazone.

Because the variation in activation energy between ligands is much smaller, interpretation of the differences in activation energy should be treated with caution. Nevertheless, the distinctly lower activation energy for the methoxy-substituted grid is consistent with an electronic effect resulting from the edge-to-face interaction between the phenyl ring and the neighbouring hydrazones at the transition state. Similar substituent effects have been noted in the dynamic behaviour of cyclophanes where it was

noted that substituents remote to the hydrogen impinging on a neighbouring aromatic ring can substantially change the rate constant (*24*). Substituent-induced changes in electron density at interacting hydrogen atoms can modify the repulsion between interacting groups – reduced electron density reduces the energy of the interaction and vice versa. In this particular case, inspection of models and the crystal structures shows that the major point of interaction is between the imine nitrogen of the hydrazone group and the *meta*-position of the phenyl ring to the substituent. Hammett σ_m constants indicate that for the methoxy ligand this position is electron deficient ($\sigma_m = +0.11$) compared to the phenyl ring; thus, the lower activation energy for the methoxy group is consistent with this model. For the dimethylamino group, the position is electron rich ($\sigma_m = -0.16$), but the difference in activation enthalpy between the phenyl and dimethylamino substituents is less than the experimental error. We note, however, that the transition state for the rotation in the dimethylamino case benefits from restored conjugation between the dimethylamino group and pyrimidine ring that could counter the effect of increased repulsion with the neighbouring ligands.

Conclusion

Taken together, our observations paint a somewhat different picture of these grid complexes than that obtained by crystal structures. The central pyrimidine may be substantially dissociated in solution with the position of the equilibrium dependent upon both the hydrazone and the electron density of the intercalated phenyl ring. The phenyl ring is able to rotate, though the neighbouring ligands still provide a significant barrier to rotation. The molecule is overall quite dynamic, explaining both the rapid self-assembly observed in most of these systems and their suitability for the formation of dynamic combinatorial libraries. Understanding the combined effects of protonation, substituents on the intercalated phenyl ring and orientation of the hydrazone should help in the design of new ligands and libraries and prediction of their properties and selectivities. In particular, the influence of phenyl substituents upon the association of the complex has the potential to control the assembly of more complex systems with more than one ligand. We are currently working on developing such systems.

Acknowledgements

This work was supported, in part, by the Petroleum Research Fund (grant 39,923-B1 to DJRB), Santa Clara University and San José State University. We thank Charles Campana for additional assistance with the solution of X-ray diffraction data.

References

(1) Lehn, J.M. *Chem. Soc. Rev.* **2007**, *36*, 151–160.
(2) Stadler, A.-M.; Kyritsakas, N.; Graff, R.; Lehn, J.-M. *Chem. Eur. J.* **2006**, *12*, 4503–4522.
(3) Ramírez, J.; Stadler, A.-M.; Kyritsakas, N.; Lehn, J.-M. *Chem. Commun.* **2007**, 237–239.
(4) Giuseppone, N.; Schmitt, J.L.; Allouche, L.; Lehn, J.M. *Angew. Chem. Int. Ed.* **2008**, *47*, 2235–2239.
(5) Giuseppone, N.; Schmitt, J.L.; Lehn, J.M. *J. Am. Chem. Soc.* **2006**, *128*, 16748–16763.
(6) Wu, A.; Isaacs, L. *J. Am. Chem. Soc.* **2003**, *125*, 4831–4835.
(7) Zheng, Y.R.; Stang, P.J. *J. Am. Chem. Soc.* **2009**, *131*, 3487– + .
(8) Barrett, E.S.; Dale, T.J.; Rebek, J. *J. Am. Chem. Soc.* **2008**, *130*, 2344–2350.
(9) Barrett, E.S.; Dale, T.J.; Rebek, J. *J. Am. Chem. Soc.* **2007**, *129*, 8818–8824.
(10) Barrett, E.S.; Dale, T.J.; Rebek, J. *J. Am. Chem. Soc.* **2007**, *129*, 3818–3819.
(11) Rojo, J.; Romero-Salguero, F.J.; Lehn, J.M.; Baum, G.; Fenske, D. *Eur. J. Inorg. Chem.* **1999**, 1421–1428.
(12) Ruben, M.; Rojo, J.; Romero-Salguero, F.J.; Uppadine, L.H.; Lehn, J.-M. *Angew. Chem. Int. Ed.* **2004**, *43*, 3644–3662.
(13) Wood, A.; Aris, W.; Brook, D.J.R. *Inorg. Chem.* **2004**, *43*, 8355–8360.
(14) Barboiu, M.; Ruben, M.; Blasen, G.; Kyritsakas, N.; Chacko, E.; Dutta, M.; Radekovich, O.; Lenton, K.; Brook, D.J.R.; Lehn, J.M. *Eur. J. Inorg. Chem.* **2006**, 784–792.
(15) Uppadine, L.H.; Gisselbrecht, J.P.; Lehn, J.M. *Chem. Commun.* **2004**, 718–719.
(16) Uppadine, L.H.; Lehn, J.M. *Angew. Chem. Int. Ed.* **2004**, *43*, 240–243.
(17) Braun, S.; Kalinowski, H.-O.; Berger, S. *150 and More Basic NMR Experiments*; Wiley-VCH: Weinheim, 1998; pp 136–143.
(18) Vlad, G.; Horvath, I.T. *J. Org. Chem.* **2002**, *67*, 6550–6552.
(19) Ruben, M.; Lehn, J.M.; Vaughan, G. *Chem. Commun.* **2003**, 1338–1339.
(20) Reich, H.J. *J. Chem. Educ. Software* **1996**, 3D2.
(21) Veshtort, M.; Griffin, R.G.J. *Magn. Reson.* **2006**, *178*, 248–282.
(22) Spek, A.L. *Acta Cryst.* **2009**, D65, 148–155.
(23) Glasson, C.R.K.; Lindoy, L.F.; Meehan, G.V. *Coord. Chem. Rev.* **2008**, *252*, 940–963.
(24) Sherrod, S.A.; Da Costa, R.L.; Barnes, R.A.; Boekelheide, V. *J. Am. Chem. Soc.* **1974**, *96*, 1565–1577.

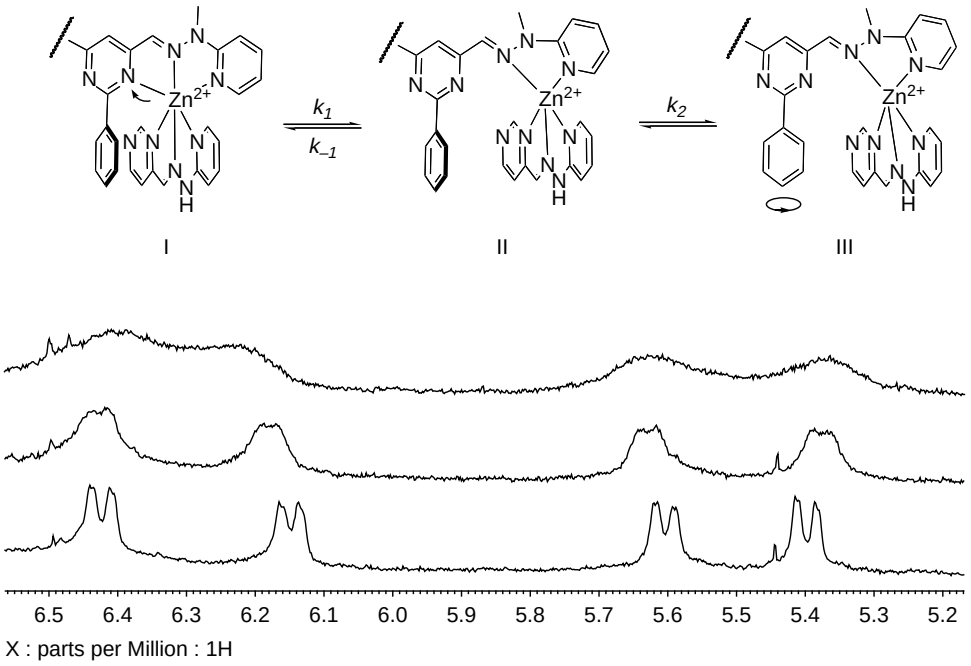

Manisha Dutta, Meisam Movassat, David J.R. Brook, Allen Oliver and Don Ward

Molecular motion in zinc hydrazone grid complexes

632–643